

Received August 9, 2019, accepted August 14, 2019, date of publication August 23, 2019, date of current version September 11, 2019.

Digital Object Identifier 10.1109/ACCESS.2019.2937191

# A Dual-Loop Control Approach of Active Magnetic Bearing System for Rotor Tracking Control

XUAN YAO<sup>1</sup>, ZHAOBO CHEN, AND YINGHOU JIAO

School of Mechatronics Engineering, Harbin Institute of Technology, Harbin 150001, China

Corresponding author: Zhaobo Chen (chenzb@hit.edu.cn)

This work was supported in part by the National Natural Science Foundation of China under Grant 11772103.

**ABSTRACT** Rotor tracking control, which can be implemented by active magnetic bearing (AMB) system with high precision, can realize many functions, such as attitude control and special surface processing. However, large-motion rotor tracking control is difficult to implement, due to AMB's highly nonlinear characteristics. In this paper, a dual-loop neural network sliding mode control (DL-NNSMC) system of AMB is proposed for rotor radial tracking control. The complete model of the AMB system is established and the dual-loop control system is designed. A circuit model that considers the rotor motion is established and the model-based inner loop of current control is established, conjointly for dealing with the influence of rotor motion on the current response and the unknown characteristics of the power amplifier. In the outer loop, a nonlinear electromagnetic force model is applied and a wavelet neural network sliding mode control algorithm is designed for accurate position control. Two cases of rotor trajectory tracking are simulated, and the simulation results demonstrate the validity of the proposed control system for large-motion rotor tracking control and its far superior control performance in terms of precision compared with common approaches based on sliding mode control (SMC).

**INDEX TERMS** Active magnetic bearing, rotor tracking control, control system design, AMB system modeling, sliding mode control.

## I. INTRODUCTION

Active magnetic bearing (AMB), which is a typical mechatronic system, realizes the stable suspension of a rotor via the active control of the electromagnet current. Benefiting from its features of no contact, no friction and active control, AMB has many advantages over conventional bearings, such as higher rotational speed, longer life, application in vacuum environments and vibration control [1]. Therefore, AMB has wide applications in turbo-machinery, precision processing tools, flywheel systems and medical devices [2].

AMB is an open-loop unstable nonlinear system due to its working principle and electromagnetic characteristics. Therefore, the control system is the core of AMB. Various control strategies have been applied in the control of AMB systems. Presently, linear methods such as PID control/adaptive PID control [3], robust control including robust nonlinear control [4], [5], optimal control like LQR control [6] are widely used. With the development of modern control theory, nonlinear

methods such as sliding mode control [7], model-based control such as internal model control [8], and fuzzy logic control [9], along with intelligent algorithms such as neural networks [10] and genetic algorithms [11], have expanding applications in AMB control. Furthermore, hybrids of different control methods [12], [13] combine the respective advantages and improve the performance of the controllers.

Due to the active control characteristic of AMB, it is possible to control the rotor trajectory, in contrast to conventional mechanical bearing support. Rotor tracking control has bright prospects in applications of rotor attitude control, active vibration control and special surface processing. Nevertheless, little research on this subject has been conducted. Chen and Kuo [14] developed a neural network intelligent sliding-mode controller for magnetic levitation systems for realizing the positioning tracking of a steel ball and experiments on the step motion demonstrated its effect. Minihan *et al.* [15] compared the control performances of controllers that are based on fuzzy logic, sliding mode, and direct linearization on tracking the sinusoidal motion of a thrust active magnetic bearing (TAMB). Although the simulation results

The associate editor coordinating the review of this article and approving it for publication was Xiaodong Sun.

demonstrated that fuzzy logic control and sliding mode control did not perform better, the model was too simple to reflect the actual scenario and the control method was basic. Smirnov *et al.* [16] and Pesch *et al.* [17] studied magnetic bearing spindle tool tracking using PID and  $\mu$ -synthesis control. They realized the tracking control of 30  $\mu\text{m}$  axial motion. The performance was satisfactory, however, the motion range was limited. Lin *et al.* [18] and [20] and Chen and Lin [19] investigated much on the tracking control of TAMB. They applied advanced complex control algorithms that are based on sliding mode control, neural network method and their hybrids, and they designed several controllers, thereby realizing the tracking control of a 1-DOF AMB system. Comparing the experimental results of rotor step motion and sinusoidal motion, their proposed controllers had higher precision than PID control and the common sliding mode control, and the controller based on nonsingular terminal sliding mode control with a recurrent Hermite neural network performed the best. Grochmal and Lynch [21] proposed a dual-layer closed-loop control system with a nonlinear reduced-order disturbance observer, and the experimental results demonstrated accurate tracking control of a 5-DOF rotor system.

Regarding the application objective, most existing research considers TAMB, which is only a single-DOF system. Whereas the radial dynamics of rotor, which may achieve novel functions, includes nonlinear disturbance and coupling, thereby rendering the tracking control more challenging. Regarding control system design, AMBs operate in strong nonlinear fields to realize large rotor motion, and the large motion of the rotor strongly influences the current response. Few studies focus on these aspects, thus the control effect is realized with limited range of rotor motion and limited running precision.

In this study, a dual-loop control system (DL-NNSMC) for rotor tracking control of a 4-DOF AMB system is proposed. In Section II, the model of an AMB-rotor system is established. A circuit model in which the rotor motion is considered for solving the nonlinear response of AMB circuit caused by rotor's large motion, and a nonlinear model of the electromagnetic actuator instead of linearized forms is used to solve for the control current. In Section III, the integral control system is designed. The control system consists of two closed loops: an inner loop for current control and an outer loop for position control. A wavelet neural network is used to identify and compensate the unknowns of the system. In Section IV, rotor motions of various trajectories are calculated via simulation (considering the rotor static imbalance, periodic disturbances and the hydrodynamic seal) and the control performance of the proposed control system is discussed. Finally, conclusions are drawn in Section V.

## II. AMB-ROTOR SYSTEM MODELING

The rotor of the AMB-rotor system has 5 DOFs. The support system consists of 2 radial magnetic bearings and 1 axial thrust magnetic bearing. In addition, there are 2 auxiliary mechanical bearings utilized only in case of AMB failure to

protect the system. Since the axial translation DOF of the rotor is controlled by the thrust magnetic bearing and it is nearly decoupled from the other DOFs, the axial motion is not considered in this study. The rotor tracking control of a 4-DOF AMB-rotor system is studied.

An AMB typically consists of 4 parts: a controller, electromagnetic actuators, power amplifiers and sensors. In this section, the AMB-rotor system is decomposed into a subsystem of rotor and electromagnetic actuators, a subsystem of power amplifiers and circuit, and a subsystem of sensors and signal processing devices, and corresponding models are established.

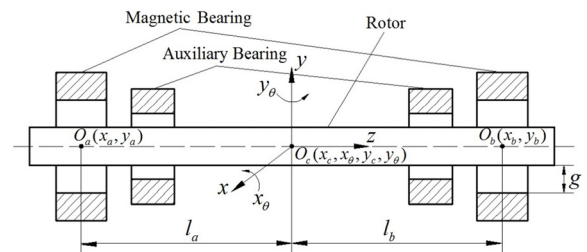


FIGURE 1. Schematic diagram of a 4-DOF AMB-rigid rotor system.

### A. ROTOR DYNAMICS

The schematic of a 4-DOF AMB-rotor system is shown in Figure 1. Ignoring rotor deformation, and considering gravity and gyroscopic effect, the dynamic model of 4-DOF AMB-rigid rotor system can be described as

$$\begin{aligned} M\ddot{\mathbf{x}}_c + G\dot{\mathbf{x}}_c &= B\mathbf{F}_b + \mathbf{F}_r + \mathbf{F}_d \\ \mathbf{x} &= T \cdot \mathbf{x}_c \end{aligned} \quad (1)$$

where,  $\mathbf{x}_c = [x_c, x_\theta, y_c, y_\theta]^T$  is the coordinate of the rotor center,  $\mathbf{x} = [x_a, x_b, y_a, y_b]^T$  is the rotor displacement vector at the AMB position,  $M$  is the mass matrix,  $G$  is the gyroscopic matrix,  $F_b$  is the active control forces of AMBs,  $F_r$  is the known forces such as gravity and unbalancing forces,  $F_d$  is the unknown forces such as periodic disturbances and the hydrodynamic seal force, and  $B$  and  $T$  are transformation matrices.

$$\begin{aligned} M &= \begin{bmatrix} m & 0 & 0 & 0 \\ 0 & I_x & 0 & 0 \\ 0 & 0 & m & 0 \\ 0 & 0 & 0 & I_y \end{bmatrix}, & G &= \begin{bmatrix} 0 & 0 & 0 & 0 \\ 0 & 0 & 0 & -I_z\omega \\ 0 & 0 & 0 & 0 \\ 0 & -I_z\omega & 0 & 0 \end{bmatrix}, \\ B &= \begin{bmatrix} 1 & 1 & 0 & 0 \\ 0 & 0 & -l_a & l_b \\ 0 & 0 & 1 & 1 \\ -l_a & l_b & 0 & 0 \end{bmatrix}, & T &= \begin{bmatrix} 1 & 0 & 0 & l_a \\ 1 & 0 & 0 & -l_b \\ 0 & -l_a & 1 & 0 \\ 0 & l_b & 1 & 0 \end{bmatrix}, \\ \mathbf{F}_r &= [e_r m \omega^2 \cos(\omega t), \quad 0, \quad e_r m \omega^2 \sin(\omega t) - mg, \quad 0]^T, \end{aligned}$$

the parameters included are given in Table 1.)

The magnetic force on each pole can be described as [1]

$$F_m = \frac{1}{4} \mu_0 N^2 A_a \left(\frac{i}{g}\right)^2 = k \left(\frac{i}{g}\right)^2 \quad (2)$$

TABLE 1. Parameters of AMB-rotor system.

Symbol	Quantity	Value
$m$	Mass of rotor	2 kg
$D$	Rotor diameter	0.04 m
$L$	Total length	0.28 m
$n$	Rotor speed	30,000 r/min
$\omega$	Rotor angular velocity	1000 $\pi$ rad/s
$l_a$	Distance between bearing a and rotor barycenter	0.1 m
$l_b$	Distance between bearing b and rotor barycenter	0.1 m
$I_x$	Rotary inertia of axis x	0.02 kg·m <sup>2</sup>
$I_y$	Rotary inertia of axis y	0.02 kg·m <sup>2</sup>
$I_z$	Rotary inertia of axis z	0.001 kg·m <sup>2</sup>
$e_r$	Eccentric errors	2×10 <sup>-6</sup> m
$g_0$	Rated air gap	8×10 <sup>-4</sup> m
$R$	Coil resistance	2.5 $\Omega$
$k$	Constant of magnetic force	3.4×10 <sup>-6</sup> N·m <sup>2</sup> /A <sup>2</sup>
$\alpha$	Angle of pole	22.5 °
$i_0$	Bias current	4 A

where,  $\mu_0$  is the permeability of vacuum,  $N$  is the number of turns of the coil,  $A_a$  is the cross-sectional area of the pole,  $i$  is the current,  $g$  is the air gap, and  $k$  is the electromagnetic coefficient.

The AMBs are differential-driven, hence, the magnetic force in each direction is:

$$F_b = k \cos \alpha \left[ \left( \frac{i_0 - i_c}{g_0 - x} \right)^2 - \left( \frac{i_0 + i_c}{g_0 + x} \right)^2 \right] \quad (3)$$

where,  $\alpha$  is the angle of the pole,  $i_0$  is the bias current,  $i_c$  is the control current,  $x$  is the rotor displacement at the AMB position, and  $g_0$  is the rated air gap. The control current  $i_c$  is the input of the AMB-rotor system and the core variable of control systems.

For conventional control of AMB,  $x \ll g_0$ , (3) can be linearized as

$$F_b = k \cos \alpha \left( \frac{4i_0^2}{g_0^3} x - \frac{4i_0}{g_0^2} i_c \right) = k_s x - k_i i_c \quad (4)$$

where,  $k_s$  is the displacement coefficient and  $k_i$  is the current coefficient.

### B. MODEL OF POWER AMPLIFIERS AND CIRCUIT

The power amplifier is typically regarded as a transconductance device with limited bandwidth, meaning that its output current is linear with the voltage. Thus, it is usually ignored or described as a simplified linear model.

However, the radial rotor motion changes the magnetic flux, and the induced voltage influences the current response characteristics. For conventional control of AMB, rotor radial motion can be ignored since its displacement and velocity

are very slight. However, for rotor tracking control, the large-amplitude and high-frequency radial motion of rotor can have a strong impact on the current response, which results in a sharp decrease in the total control performance. Therefore, a model of power amplifiers and circuit that considers the rotor motion is derived and established in this section.

The power amplifier circuit is expressed as

$$U = Ri + U_L = Ri + d \frac{Li}{dt} \quad (5)$$

where,  $U$  is the voltage of the power amplifier,  $U_L$  is the induced voltage of inductance,  $R$  is the coil resistance, and  $L$  is the inductance.

According to

$$L = \frac{N\Phi}{i} \quad (6)$$

$$\Phi = BA_a = \frac{\mu_0 Ni A_a}{2g} = \frac{2k \cdot i}{N \cdot g} \quad (7)$$

where,  $\Phi$  is the magnetic flux and  $B$  is the magnetic induction intensity,

By substituting (6), (7) into (5), we obtain

$$\begin{aligned} U &= Ri + Nd \frac{\Phi}{dt} = Ri + \frac{d}{dt} \left( \frac{2ki}{g} \right) \\ &= Ri + \frac{2k}{g} \frac{di}{dt} - \frac{2ki}{g^2} \frac{dg}{dt} \end{aligned} \quad (8)$$

Thus the model of the power amplifier circuit in each direction is

$$\begin{cases} K_c(i_0 - i_c) = Ri_1 + \frac{2k}{g_0 - x} \frac{di_1}{dt} + \frac{2ki_1}{(g_0 - x)^2} \frac{dx}{dt} \\ K_c(i_0 + i_c) = Ri_2 + \frac{2k}{g_0 + x} \frac{di_2}{dt} - \frac{2ki_2}{(g_0 + x)^2} \frac{dx}{dt} \end{cases} \quad (9)$$

where,  $K_c$  is the input gain of the power amplifier.

It's obvious that the actual currents  $i_1, i_2$  are far from the assumed form  $i_0 \pm i_c$  when  $x$  changes substantially.

### C. MODEL OF SENSORS AND SIGNAL PROCESSING DEVICES

Displacement sensors are used in AMBs for data measurement and feedback. Assuming that the sensors have fixed gain and bandwidth, the sensors can be regarded as simple first-order low-pass filter.

To avoid the aliasing of signals, anti-aliasing filters that act on the input signal are typically utilized. Anti-aliasing filters can also be regarded as a first-order low-pass filter.

In addition, digital controllers introduce time delay between signal sampling and instruction output, which is typically approximately one to two sample intervals.

Therefore, the sensors, anti-aliasing filters, and the sample delay of controller are merged to form a delayed module with the model

$$\frac{d}{dt} x_{in} + \frac{1}{\tau} x_{in} = \frac{K_{SC}}{\tau} x \quad (10)$$

where,  $x$  is the displacement detected by the sensors,  $x_{in}$  is the input signal of controller,  $\tau$  is a time constant, which is

the sum of time delay of sensors and anti-aliasing filters, and sample delay of the controller, and  $K_{SC}$  is the overall gain between sensors and the controller.

### III. CONTROL SYSTEM DESIGN

#### A. STRUCTURE OF PROPOSED CONTROL SYSTEM

For the AMB control system, closed-loop control is necessary due to its open-loop unstable characteristics. As the rotor position is the objective and the current is the approach, simultaneous control of the two variables is adopted. The integrated control system (dual-loop neural network sliding mode control, DL-NNSMC) consists of the position closed-loop control (the outer loop) and the current closed-loop control (the inner loop). In the current control, since the rotor motion has a substantial impact on the current response and the characteristics of power amplifiers are usually unknown, a model-based sliding mode controller is configured. In the position control, wavelet neural network sliding mode control (WNNSMC) is applied. As discussed in Introduction, the nonlinear characteristics, high robustness demand, and complicated dynamics of the system are the key problems. Sliding mode control (SMC) has the advantages of nonlinear control algorithm and good global robustness, and wavelet neural networks perform excellently at compensation control. So WNNSMC, the combination of the two methods with respective advantages, is well fit for this work.

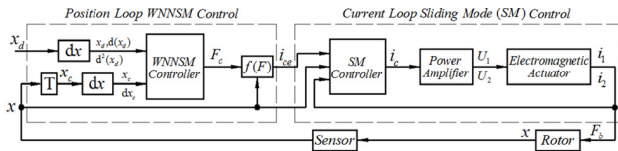


FIGURE 2. Block diagram of AMB control system.

The block diagram of the control system is presented in Figure 2. Its operational process is described as follows. The rotor displacement at the AMB position ( $x$ ) obtained by the sensors and the expected rotor trajectory ( $x_{cd}$ ) are inputted into the control system. First, the displacement of the rotor axle center ( $x_c$ ) is calculated via transformation matrix  $T$ . Second, the expected velocity, the expected acceleration and the actual velocity of rotor axle center are calculated. Next, in the position loop sliding mode controller, the required magnetic force ( $F_c$ ) is calculated and then the control current ( $i_{ce}$ ) is solved by (31). Then the actual control current ( $i_c$ ) is outputted through the current loop controller calculated via  $i_{ce}$  and feedback pole currents ( $i_1, i_2$ ). Last, the power amplifier translates  $i_c$  to the pole voltage to generate the control force ( $F_b$ ) acting on the rotor.

#### B. NEURAL NETWORK SLIDING MODE CONTROL

For the controlled system

$$m\ddot{x} = u(t) + f(x, \dot{x}, t) + d(x, \dot{x}, t) \quad (11)$$

where,  $u, f$  and  $d$  are the control force, the known forces and unknown forces, respectively.

The sliding surface is defined by the position error ( $e = x_d - x$ , where  $x_d$  is the desired displacement) and velocity error as

$$s(t) = ce(t) + \dot{e}(t) \quad (12)$$

Neural network is an effective approach for improving control accuracy of mechanical system and had been applied in many forms in AMB control [22]. Wavelet neural network, which has excellent nonlinear approximation ability [23], is joint in the sliding mode control for online identification and compensation control for reducing the position error.

The wavelet neural network consists of 3 parts: the input layer, the hidden layer and the output layer. The structure of the  $m$ - $n$ -1 form wavelet neural network is illustrated in Figure 3.

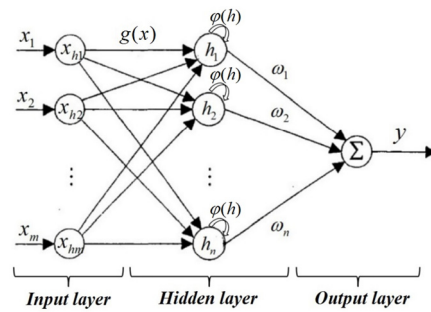


FIGURE 3. Structure of the  $m$ - $n$ -1 wavelet neural network.

The operational process of neurons in the hidden layer is

$$h_j = g(x_h) = \sum_{i=1}^m \frac{x_{hi} - b_{ij}}{a_{ij}} \quad j = 1, 2, \dots, n \quad (13)$$

where,  $a_{ij}$  is the scale coefficient and  $b_{ij}$  is the shift coefficient.

The activation function of neurons can be different wavelet functions. The Mexican hat function and the Morlet function are commonly used due to their simple expressions as well as good localization and symmetry feature in the time and frequency domain [24]. Here the Mexican hat function is used as activation function  $\phi$  :

$$\phi(h) = (1 - h^2) \exp(-\frac{h^2}{2}) \quad (14)$$

The output of the neural network is

$$u_{NN} = y = \omega^T \cdot \phi(h) \quad (15)$$

where,  $\omega$  is the weights of neurons, and  $\omega = [\omega_1, \omega_2, \dots, \omega_n]^T$ .

The objective function of the network is constructed based on the sliding surface to maintain the stability of the combined control system and to reduce the error:

$$E_{NN} = s \cdot \dot{s} \quad (16)$$

where,  $\dot{s}$  is the derivative of  $s$  :

$$\begin{aligned} \dot{s} &= \dot{c}\dot{e}(t) + \ddot{e}(t) = \dot{c}\dot{e}(t) + \ddot{x} - \ddot{x}_d \\ &= \dot{c}\dot{e}(t) - \ddot{x}_d + \frac{1}{m}(u(t) + f(x, \dot{x}, t) + d(x, \dot{x}, t)) \end{aligned} \quad (17)$$

The weights of the neurons are updated via the gradient descent method:

$$\begin{aligned} \dot{\omega} &= -\gamma_0 \frac{\partial E_{NN}}{\partial \omega} = -\gamma_0 \frac{\partial (s \cdot \dot{s})}{\partial u(t)} \frac{\partial u(t)}{\partial \omega} \\ &= -\gamma_0 \cdot s \cdot \frac{\partial \dot{s}}{\partial u(t)} \frac{\partial u_{NN}(t)}{\partial \omega} = \frac{\gamma_0}{m} \cdot s \cdot \frac{\partial u_{NN}(t)}{\partial \omega} \\ &= \gamma \cdot s \cdot \phi(\mathbf{h}) \end{aligned} \quad (18)$$

where,  $\gamma_0$  is a learning coefficient, and  $\gamma$  is the learning rate of the neural network, which satisfies  $\gamma > 0$ .

The unknown disturbance is approximated by the neural network [25]:

$$d(x, \dot{x}, t) = \omega^{*T} \cdot \phi(\mathbf{h}) + \varepsilon \quad (19)$$

where,  $\omega^*$  is the ideal weights of the neural network, and  $\varepsilon$  is the ideal approximation error, which satisfies  $|\varepsilon| \leq \varepsilon_N$ .

Thus, the approximation error of the neural network is

$$\begin{aligned} d(x, \dot{x}, t) - u_{NN}(t) &= \omega^{*T} \cdot \phi(\mathbf{h}) + \varepsilon - \omega^T \cdot \phi(\mathbf{h}) \\ &= -\tilde{\omega}^T \cdot \phi(\mathbf{h}) + \varepsilon \end{aligned} \quad (20)$$

The output of the neural network sliding mode controller can be expressed as

$$\begin{aligned} u(t) &= u_{SM}(t) - u_{NN}(t) + u_{SG}(t) \\ u_{SM}(t) &= m[\ddot{x}_d(t) - c\dot{e}(t)] - f(x, \dot{x}, t) \\ u_{NN}(t) &= \omega^T \cdot \phi(\mathbf{h}) \\ u_{SG}(t) &= -k_a \cdot s - \delta \cdot \text{sat}(s), \quad k_a > 0, \delta > 0 \end{aligned} \quad (21)$$

where,  $u_{SM}(t)$  is the sliding mode control term,  $u_{NN}(t)$  is the neural network control term,  $u_{SG}(t)$  is the switching control term, and  $k_a, \delta$  are the gains.

In the switching control term  $u_{SG}(t)$ , the exponential approach law and quasi-sliding mode method are applied to reduce chattering [26].

$$\text{sat}(s) = \begin{cases} 1, & s > \Delta \\ s/\Delta, & |s| \leq \Delta \\ -1, & s < -\Delta \end{cases} \quad (22)$$

where,  $\Delta$  is the width of the boundary layer.

Proof of the stability of the system: Based on the Lyapunov stability theorem, the Lyapunov function is defined as

$$V = \frac{1}{2}s^2 + \frac{1}{2m\gamma}\tilde{\omega}^T\tilde{\omega} \quad (23)$$

Thus,

$$\dot{V} = s \cdot \dot{s} + \frac{1}{m\gamma}\tilde{\omega}^T\dot{\tilde{\omega}} \quad (24)$$

Substituting (17), (20), and (21) into (24) yields

$$\begin{aligned} \dot{V} &= s \cdot \dot{s} + \frac{1}{m\gamma}\tilde{\omega}^T\dot{\tilde{\omega}} \\ &= s \cdot \frac{1}{m}(d(t) - u_{NN}(t) - k_a \cdot s - \delta \cdot \text{sat}(s)) + \frac{1}{m\gamma}\tilde{\omega}^T\dot{\tilde{\omega}} \\ &= \frac{1}{m}(-k_a \cdot s^2 - \delta \cdot s \cdot \text{sat}(s) + \varepsilon \cdot s) \end{aligned} \quad (25)$$

Set  $\delta > \varepsilon_N$ , and outside of the boundary layer, we can obtain

$$\dot{V} = \frac{1}{m}(-k_a \cdot s^2 - (\delta - \varepsilon)|s|) < -\frac{k_a}{m}s^2 < 0 \quad (26)$$

According to (26), the system is Lyapunov stable within a small neighborhood of the sliding surface. Therefore the stability of the system is guaranteed [26].

### C. DESIGN OF THE POSITION SLIDING MODE CONTROLLER

The sliding surface is set according to the position error and the velocity error of the rotor center

$$s(\mathbf{x}_c) = c\mathbf{e}_c + \dot{\mathbf{e}}_c \quad (27)$$

The neural network compensation control is set only in the 2 translation DOFs to simplify the control system. The structure of the neural network is 4-9-2 and its inputs are the nondimensionalized displacement and velocity of the rotor axle center. The output of the neural network is

$$\mathbf{u}_{NNW} = [\omega_1^T \cdot \phi(\mathbf{h}_1), \quad 0, \quad \omega_2^T \cdot \phi(\mathbf{h}_2), \quad 0]^T \quad (28)$$

A strategy of subsection control is applied to avoid the huge jitter that is caused by the online adjustment of neural network weights in the initial control if the error is large. The neural network is set offline when the error is large, hence, the output of neural network control can be expressed as

$$\begin{cases} \mathbf{u}_{NN}(t) = 0, & s > 5\Delta \\ \mathbf{u}_{NN}(t) = \mathbf{u}_{NNW}(t), & s \leq 5\Delta \end{cases} \quad (29)$$

The output of the position sliding mode controller (required magnetic force) is expressed as

$$\mathbf{F}_c = \mathbf{u}(t) = \mathbf{B}^{-1} \cdot [\mathbf{M} \cdot (\ddot{\mathbf{x}}_{cd} - c\dot{\mathbf{e}} - \delta_1 \cdot \text{sat}(s) - k_a \cdot s) + \mathbf{G} \cdot \dot{\mathbf{x}}_c - \mathbf{F}_r - \mathbf{u}_{NN}] \quad (30)$$

The magnetic force is described as a nonlinear model instead of a linearization. The control current is directly solved by (3) and the amplitude of the output is limited. Thus the control current in each direction can be obtained as

$$i_c = \begin{cases} -\frac{g_0^2}{4ki_0}, & x = 0 \\ \frac{(g_0^2 + x^2)i_0}{2g_0x}, & \\ x \cdot (F_c + \frac{k \cos \alpha (g_0^2 - x^2)^2 i_0^2}{g_0x(g_0 - x)^2 (g_0 + x)^2}) < 0 \\ \frac{i_0}{2g_0x} [(g_0^2 + x^2) - (g_0^2 - x^2) \sqrt{1 + \frac{g_0x}{i_0^2} \cdot \frac{F_c}{k}}], & \text{others} \end{cases} \quad (31)$$

The final output of the position loop controller is  $i_{ce} = [i_{cexa}, i_{cexb}, i_{ceya}, i_{ceyb}]^T$ .



**D. DESIGN OF THE CURRENT SLIDING MODE CONTROLLER**

The controller is based on the circuit model. Define  $i_{ca} = (i_2 - i_1)/2$ . From (9) we obtain

$$i_c \approx i_{ca} + \frac{2k}{Rg_0} \dot{i}_{ca} - \frac{2ki_0}{Rg_0^2} \dot{x} \quad (32)$$

The sliding surface is set as

$$\begin{aligned} s_i &= e_i = i_{ca} - \dot{i}_{ce} \\ \dot{s}_i &= \dot{e}_i = \dot{i}_{ca} - \ddot{i}_{ce} = -\delta_2 \cdot \text{sat}(s_i) \end{aligned} \quad (33)$$

Hence, the output of the current loop controller is

$$i_c = i_{ca} + \frac{2k}{Rg_0} (\dot{i}_{ce} - \delta_2 \cdot \text{sat}(s_i)) - \frac{2ki_0}{Rg_0^2} \dot{x} \quad (34)$$

**IV. SIMULATION ANALYSIS**

**A. PARAMETER SETTINGS**

The main parameters of the AMB-rotor system are listed in Table 1.

The unknown disturbance in the simulation is set as

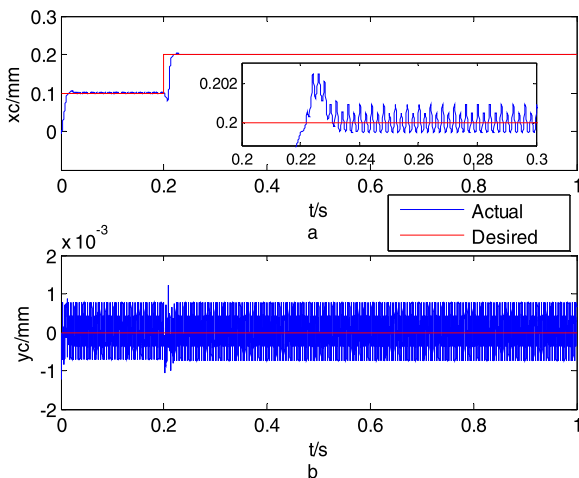
$$F_d = T_d \cdot d(t) + F_s \quad (35)$$

where,  $d(t)$  is the periodic disturbance loaded at the rotor headend,  $T_d$  is its transformation matrix, and  $F_s$  is the hydrodynamic seal force calculated using the Muszynska model [27].

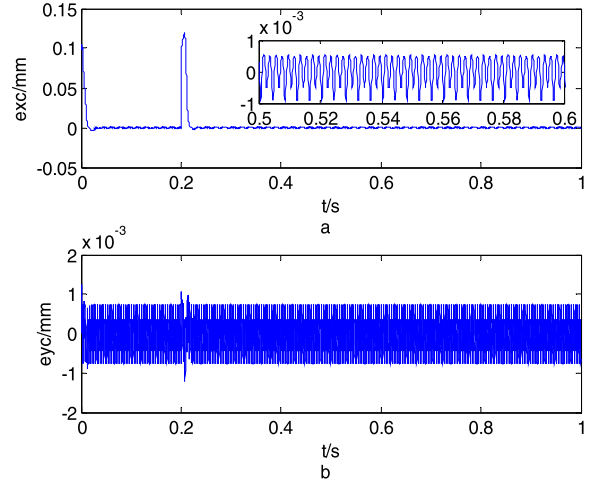
Numerical simulation is conducted with the sampling frequency of 10 kHz. Measurement noises of feedback signals and signal filtering processing are also considered.

**B. CONTROL OF THE STEP RESPONSE OF ROTOR**

Simulation of the step response in the  $x$  direction is conducted. The motion of the rotor center is plotted in Figure 4. It shows that the response of the proposed control system is very fast. The response time is less than 0.03 s without overshoot, and the vibration in the  $y$  direction remains tiny.



**FIGURE 4.** Motion of the rotor center: (a) in the  $x$  direction and (b) in the  $y$  direction.



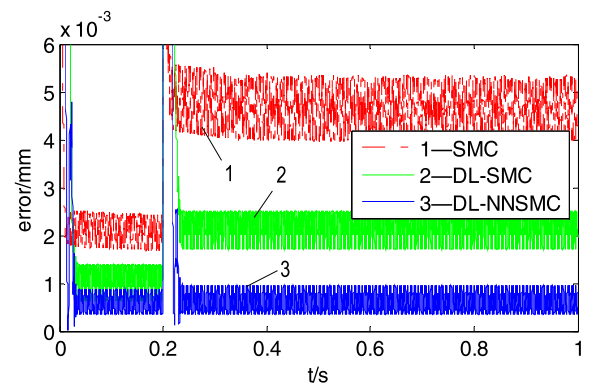
**FIGURE 5.** Rotor position at each AMB. The position error of each translation DOF: (a) in the  $x$  direction and (b) in the  $y$  direction.

Figure 5 shows the position errors in the two translation DOFs of the rotor center. The steady-state error is less than  $1 \mu\text{m}$ . The results also demonstrate that the error increases with the radial displacement becoming larger.

The position error of the rotor center is defined as

$$e_c = \sqrt{e_{xc}^2 + e_{yc}^2} \quad (36)$$

The position errors of 3 control systems are plotted in Figure 6. It is indicated that the errors of the proposed dual-loop control systems (DL-NNSMC and DL-SMC) are much smaller than the error of common SMC with a linear magnetic force model (4). Benefiting from the compensation control by the neural network, which is based on its nonlinear approximation performance, the DL-NNSMC control system realizes the highest tracking precision.



**FIGURE 6.** Error comparison of 3 controllers.

**C. CONTROL OF THE CIRCULAR TRAJECTORY OF ROTOR**

In this case, the rotor is controlled to track a 10 Hz circular trajectory. The trajectory is an involute circle from the origin and the final radius is 0.3 mm.

The trajectory diagram of the rotor center is shown in Figure 7, which indicates that the proposed control system can realize complex dynamic orbit control over a large range in the available air gap.

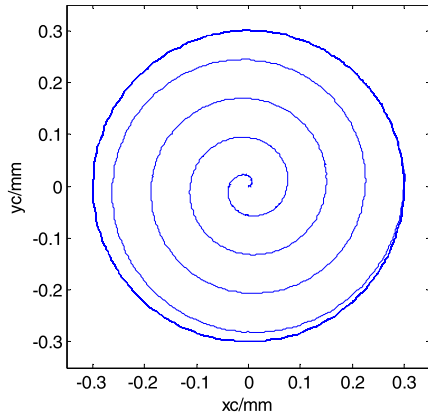


FIGURE 7. Trajectory diagram of the rotor center.

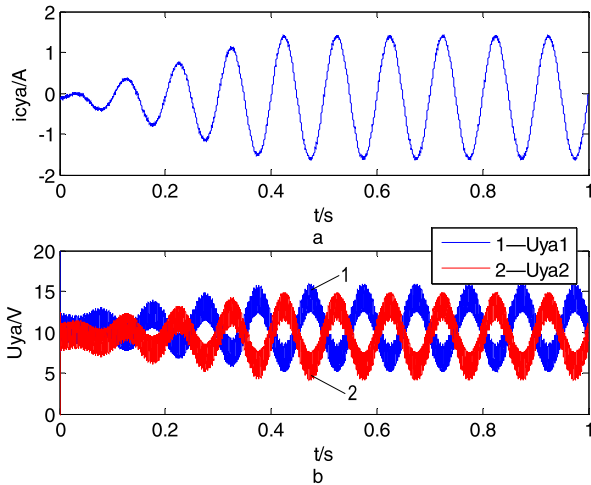


FIGURE 8. Parameters of Bearing 1 in the y direction: (a) the control current and (b) the pole voltage.

The required control current ( $i_{cya}$ ) and pole voltages ( $U_{ya1}$  &  $U_{ya2}$ ) of bearing 1 in the y direction are shown in Figure 8. Due to the influence of rotor radial motion on the current response, the pole voltages have much more large shake than the control current.

The position errors of each translation DOF, which are plotted in Figure 9, indicate good control effect in this case. The maximum position error is approximately  $9 \mu\text{m}$  (3%). Comparing with the data of the step response shown in Figure 5, the error of dynamic trajectory control is substantially larger than the error of static-state control.

Figure 10 shows the position errors of 3 control systems. Similar to the results in the case of the step response, the proposed dual-loop control systems (DL-NNSMC and DL-SMC) have much smaller error than common SMC, and the DL-NNSMC control system exhibits the best performance in terms of precision.

D. CONTROL EFFECT COMPARISON

The performance measures of the control systems in the above 2 cases are presented in Table 2, Table 3 and Figure 11. Table 2 represents the data of the second step response in

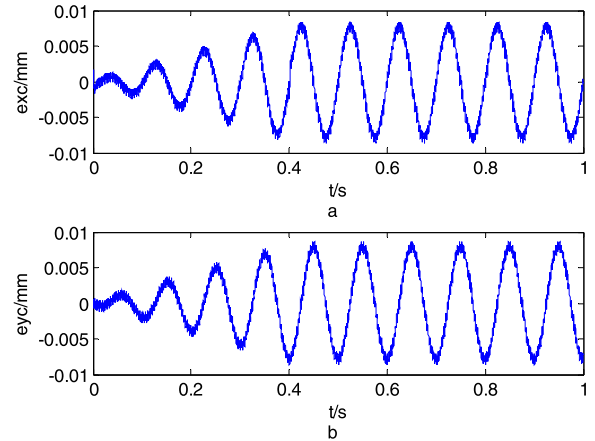


FIGURE 9. Position error of each translation DOF: (a) in the x direction, and (b) in the y direction.

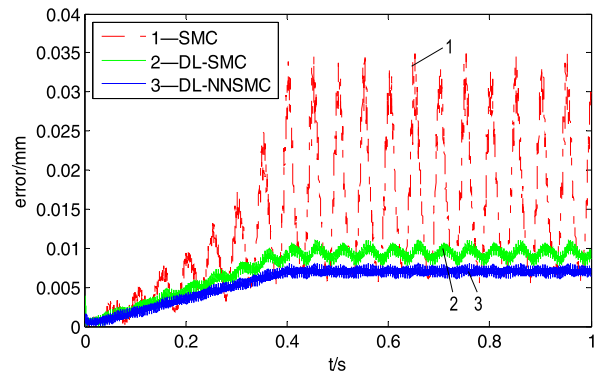


FIGURE 10. Error comparison of 3 controllers.

TABLE 2. Control effect comparison on the step response.

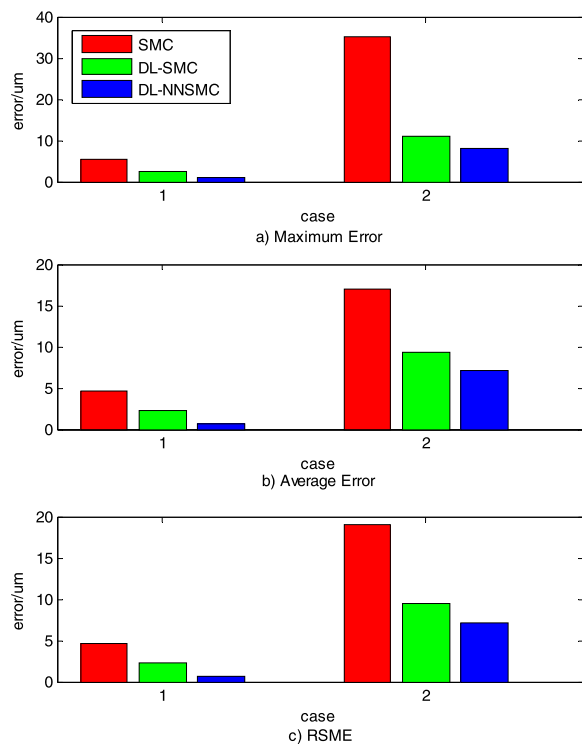
Performance	SMC	DL-SMC	DL-NNSMC
Error/m			
Maximum	$5.356 \times 10^{-6}$	$2.511 \times 10^{-6}$	$9.506 \times 10^{-7}$
Average	$4.651 \times 10^{-6}$	$2.238 \times 10^{-6}$	$6.021 \times 10^{-7}$
RMSE	$4.665 \times 10^{-6}$	$2.251 \times 10^{-6}$	$6.054 \times 10^{-7}$
Response time/s	0.02	0.03	0.03

case 1, and Table 3 represents the data of the stable circular trajectory with the final radius in case 2. The simulation results demonstrate that the proposed control system has a good effect on rotor tracking control and it substantially outperforms the common sliding mode control, especially under large dynamic motion of the rotor.

Three points are made for the results. First, the term of rotor motion in (9) improves the accuracy of the model, so that the error decreases significantly, and the special inner loop controller for the current increases the response and precision effectively. Second, the use of a nonlinear equation for the

**TABLE 3.** Control effect comparison on the circular trajectory.

Error/m	SMC	DL-SMC	DL-NNSMC
Maximum	$3.527 \times 10^{-5}$	$1.104 \times 10^{-5}$	$8.011 \times 10^{-6}$
Average	$1.697 \times 10^{-5}$	$9.387 \times 10^{-6}$	$7.061 \times 10^{-6}$
RMSE	$1.903 \times 10^{-5}$	$9.414 \times 10^{-6}$	$7.075 \times 10^{-6}$

**FIGURE 11.** Steady-state error comparison of 3 controllers in 2 cases.

magnetic force reduces the effect of the rotor position on error. According to Figure 6., the average error of SMC increases from  $2.0 \mu\text{m}$  to  $4.7 \mu\text{m}$  when rotor position changes from  $0.1 \text{ mm}$  to  $0.2 \text{ mm}$ , while the average errors of the proposed control systems less than double. Third, the wavelet neural network compensates the disturbance and uncertainties of the system efficiently, hence, the DL-NNSMC control system exhibits the best performance.

## V. CONCLUSION

Aiming at large-motion rotor tracking control of AMB systems, a dual-loop nonlinear control system is presented in this paper. The current control loop and the circuit model, which consider the rotor motion, decrease the influence of large motion of the rotor on the current response. The AMB model in the control system, which is not linearized, deals with the highly nonlinear characteristics that are introduced by large rotor motion. In the position loop, sliding mode control is applied and a wavelet neural network is added for compensation control, thereby leading to high control precision.

Finally, simulation of rotor radial trajectory tracking control on a 4-DOF AMB system is implemented in two cases, and from the results, the following conclusions are drawn: the processing of the control system is effective and thereby enables the proposed control system to realize accurate rotor trajectory tracking of large dynamic motion, and the proposed control system exhibits a substantial advantage in terms of precision for rotor tracking control under both static operation and dynamic motion.

## REFERENCES

- [1] G. Schweitzer, "Introduction and survey," in *Magnetic Bearings*. Berlin, Germany: Springer, 2009, pp.2–5.
- [2] X. Sun, L. Chen, and Z. Yang, "Overview of bearingless permanent-magnet synchronous motors," *IEEE Trans. Ind. Electron.*, vol. 60, no. 12, pp. 5528–5538, Dec. 2013.
- [3] C. Barthod and G. Lamarquand, "Degrees of freedom control of a magnetically levitated rotor," *IEEE Trans. Magn.*, vol. 31, no. 6, pp. 4202–4204, Nov. 1995.
- [4] I. S. Kuseyri, "Robust control and unbalance compensation of rotor/active magnetic bearing systems," *J. Vibrat. Control*, vol. 18, no. 6, pp. 817–832, May 2012.
- [5] A. Kuperman, "Uncertainty and disturbance estimator-assisted control of a two-axis active magnetic bearing," *Trans. Inst. Meas. Control*, vol. 38, no. 6, pp. 764–772, Jun. 2016.
- [6] S. Y. Yoon, L. Di, P. Anantachaisilp, and Z. Lin, "Truncated predictor feedback control for active magnetic bearing systems with input delay," *IEEE Trans. Control Syst. Technol.*, vol. 24, no. 6, pp. 2182–2189, Nov. 2016.
- [7] M.-J. Jang, C.-L. Chen, and Y.-M. Tsao, "Sliding mode control for active magnetic bearing system with flexible rotor," *J. Franklin Inst.*, vol. 342, no. 4, pp. 401–419, Jul. 2005.
- [8] X. Sun, Z. Shi, L. Chen, and Z. Yang, "Internal model control for a bearingless permanent magnet synchronous motor based on inverse system method," *IEEE Trans. Energy Convers.*, vol. 31, no. 4, pp. 1539–1548, Dec. 2016.
- [9] H. C. Sung, J. B. Park, Y. H. Joo, and K. C. Lin, "Robust digital implementation of fuzzy control for uncertain systems and its application to active magnetic bearing system," *Int. J. Control, Automat. Syst.*, vol. 10, no. 3, pp. 603–612, Jun. 2012.
- [10] S.-Y. Chen and F.-J. Lin, "Decentralized PID neural network control for five degree-of-freedom active magnetic bearing," *Eng. Appl. Artif. Intell.*, vol. 26, no. 3, pp. 962–973, Mar. 2013.
- [11] I. A. Griffin, A. J. Chipperfield, P. J. Fleming, C. Davies, and N. Grum, "Active magnetic bearing control system testing and validation using a multiobjective genetic algorithm," in *Proc. 26th Annu. Conf. IEEE Electron. Soc. (IECON)*, Nagoya, Japan, Oct. 2000, pp. 1675–1679.
- [12] Y. Sun, J. Xu, H. Y. Qiang, and G. B. Lin, "Adaptive neural-fuzzy robust position control scheme for maglev train systems with experimental verification," *IEEE Trans. Ind. Electron.*, vol. 66, no. 11, pp. 8589–8599, Nov. 2019.
- [13] Y. Sun, J. Xu, H. Qiang, C. Chen, and G. Lin, "Adaptive sliding mode control of maglev system based on RBF neural network minimum parameter learning method," *Measurement*, vol. 141, pp. 217–226, Jul. 2019.
- [14] S.-C. Chen and C.-Y. Kuo, "ARNISMC for MLS with global positioning tracking control," *IET Electr. Power Appl.*, vol. 12, no. 4, pp. 518–526, Apr. 2018.
- [15] T. P. Minihan, S. Lei, G. Sun, A. Palazzolo, A. F. Kascak, and T. Calvert, "Large motion tracking control for thrust magnetic bearings with fuzzy logic, sliding mode, and direct linearization," *J. Sound Vibrat.*, vol. 263, no. 3, pp. 549–567, Jun. 2003.
- [16] A. Smirnov, A. H. Pesch, O. Pyrhönen, and J. T. Sawicki, "High-precision cutting tool tracking with a magnetic bearing spindle," *J. Dyn. Syst. Meas. Control*, vol. 137, no. 5, May 2015, Art. no. 051017.
- [17] A. H. Pesch, A. Smirnov, O. Pyrhönen, and J. T. Sawicki, "Magnetic bearing spindle tool tracking through  $\mu$ -synthesis robust control," *IEEE/ASME Trans. Mechatron.*, vol. 20, no. 3, pp. 1448–1457, Jun. 2015.
- [18] F. J. Lin, S. Y. Chen, and M. S. Huang, "Tracking control of thrust active magnetic bearing system via Hermite polynomial-based recurrent neural network," *IET Electr. Power Appl.*, vol. 4, no. 9, pp. 701–714, Nov. 2010.



- [19] S.-Y. Chen and F.-J. Lin, "Robust nonsingular terminal sliding-mode control for nonlinear magnetic bearing system," *IEEE Trans. Control Syst. Technol.*, vol. 19, no. 3, pp. 636–643, May 2011.
- [20] F.-J. Lin, S.-Y. Chen, and M.-S. Huang, "Adaptive complementary sliding-mode control for thrust active magnetic bearing system," *Control Eng. Pract.*, vol. 19, no. 7, pp. 711–722, Jul. 2011.
- [21] T. R. Grochmal and A. F. Lynch, "Precision tracking of a rotating shaft with magnetic bearings by nonlinear decoupled disturbance observers," *IEEE Trans. Control Syst. Technol.*, vol. 15, no. 6, pp. 1112–1121, Nov. 2007.
- [22] X. D. Sun, B. Su, L. Chen, Z. Yang, X. Xu, and Z. Shi, "Precise control of a four degree-of-freedom permanent magnet biased active magnetic bearing system in a magnetically suspended direct-driven spindle using neural network inverse scheme," *Mech. Syst. Signal Process.*, vol. 88, pp. 36–48, May 2017.
- [23] Z.-L. Gaing, "Wavelet-based neural network for power disturbance recognition and classification," *IEEE Trans. Power Del.*, vol. 19, no. 4, pp. 1560–1568, Oct. 2004.
- [24] H. Adeli and X. Jiang, "Dynamic fuzzy wavelet neural network model for structural system identification," *J. Struct. Eng.*, vol. 132, no. 1, pp. 102–111, 2006.
- [25] J. Park and I. W. Sandberg, "Universal approximation using radial-basis-function networks," *Neural Comput.*, vol. 3, no. 2, pp. 246–257, Mar. 1991.
- [26] J. J. Slotine and S. S. Sastry, "Tracking control of non-linear systems using sliding surfaces, with application to robot manipulators," *Int. J. Control*, vol. 38, no. 2, pp. 465–492, Aug. 1983.
- [27] L. T. Tam, A. J. Przekwas, A. Muszynska, R. C. Hendricks, M. J. Braun, L. T. Tam, and R. L. Mullen, "Numerical and analytical study of fluid dynamic forces in seals and bearings," *J. Vibrat. Acoust.*, vol. 110, no. 3, pp. 112–119, 1987.



**ZHAOBO CHEN** received the Ph.D. degree in mechanical engineering from the Harbin Institute of Technology, Harbin, China, in 1995, where he is currently a Professor.

His current research interests include rotor dynamics, nonlinear dynamics, vibration control, and acoustic radiation control.



**XUAN YAO** received the B.S. degree in mechanical design, manufacturing, and automation and the M.S. degree in mechanical engineering from the Harbin Institute of Technology, in 2012 and 2014, respectively, where he is currently pursuing the Ph.D. degree in mechanical engineering.

He is also with the Noise and Vibration Control Laboratory, School of Mechatronics Engineering, Harbin Institute of Technology. His research interests include vibration control and magnetic bearing systems.



**YINGHOU JIAO** received the Ph.D. degree in mechanical engineering from the Harbin Institute of Technology, Harbin, China, in 2001, where he is currently a Professor.

His current research interests include rotor dynamics, nonlinear dynamics, fluid-induced vibration, and failure diagnosis of turbomachinery.

...